

IS THE MACRONOVA IN GW170817 POWERED BY THE CENTRAL ENGINE?

TATSUYA MATSUMOTO¹, KUNIHITO IOKA², SHOTA KISAKA^{3,4}, AND EHUD NAKAR⁵
draft v1

ABSTRACT

The gravitational wave event GW170817 from a binary neutron star (NS) merger is accompanied by electromagnetic counterparts, and the optical and near-infrared emission is called a macronova (or kilonova). Although the radioactivity of synthesized r -process elements is widely discussed as an energy source, its decisive evidence is not clearly shown yet. We discuss a macronova powered by the central engine activities such as jet activities and X-rays from the matter fallback, and show that the engine model allows much broader parameter spaces, in particular smaller ejecta mass ($\sim 10^{-4} - 0.01 M_{\odot}$) than the r -process model. The blue and red macronovae are naturally explained by various combinations of the ejecta such as a cocoon and merger ejecta with the energy sources of jets and X-rays. The required energy injection is very similar to the X-ray excess observed in GRB 130603B with the power-law slope of ~ -1.3 . The required lanthanoid fraction for the opacity can be also consistent with the Galactic one. Early or late multi-wavelength observations are crucial for revealing the central engine of short gamma-ray bursts and the r -process nucleosynthesis.

Subject headings: — —

1. INTRODUCTION

The LIGO-VIRGO collaboration detected the gravitational waves (GWs) from a binary neutron star (NS) merger for the first time (Abbott et al. 2017). NS mergers have been expected to accompany electromagnetic signals with rich physical information. Just after the GW detection, many follow-up observations in various wavelengths were performed (LIGO Scientific Collaboration, et al. 2017, and references therein). The *Fermi* and INTEGRAL satellites observed a gamma-ray signal ~ 1.7 s after the GW detection, which may reveal that some short gamma-ray bursts (sGRBs) originate from NS mergers (LIGO Scientific Collaboration, et al. 2017b; Goldstein et al. 2017; Savchenko et al. 2017). In other wavelengths such as X-ray, ultra-violet, optical, near infrared (NIR), and radio bands, electromagnetic counterparts were subsequently detected. These detections associated with the GW event open up the era of multimessenger astronomy.

In this work, we focus mainly on the counterparts in optical and NIR bands (Arcavi et al. 2017; Chornock et al. 2017; Coulter et al. 2017; Cowperthwaite et al. 2017; Díaz et al. 2017; Drout et al. 2017; Evans et al. 2017; Kasliwal et al. 2017; Kilpatrick et al. 2017; McCully et al. 2017; Nicholl et al. 2017; Pian et al. 2017; Shappee et al. 2017; Smartt et al. 2017; Soares-Santos et al. 2017; Tanvir et al. 2017; Tominaga et al. 2017; Utsumi et al. 2017; Valenti et al. 2017). The optical and NIR counterparts of GW170817,

SSS17a (or AT2017fgo), were first discovered by the Swope Supernovae Survey about half a day after the merger (Coulter et al. 2017). SSS17a showed a bright optical emission at first few days, and its spectra are well fitted by a blackbody. The bolometric luminosity and the temperature are evaluated as $L \simeq 7 \times 10^{41} \text{ erg s}^{-1}$ and $T \simeq 7000 \text{ K}$ at 1 day. Afterwards, the optical emission decayed and transitioned to an NIR emission in a week. Although the spectrum began to deviate from a blackbody, the luminosity and temperature are evaluated as $L \simeq 8 \times 10^{40} \text{ erg s}^{-1}$ and $T \simeq 3000 \text{ K}$ at 1 week.

Theoretically, an electromagnetic counterpart following a binary NS merger was predicted a few decades ago, and it was named as a macronova (Li & Paczyński 1998; Kulkarni 2005), or kilonova (Metzger et al. 2010). Binary NS mergers are one of the most promising production sites of the heavy elements (Lattimer & Schramm 1974; Symbalisty & Schramm 1982; Eichler et al. 1989). The coalescence of NSs ejects neutron-rich matter, where heavy elements are synthesized by the rapid neutron capture, so-called the r -process. The produced r -process elements are unstable and radioactively decay to heat up the ejecta, which results in optical and NIR emissions. In this work, we call this scenario as the r -process model.

In order to reproduce the SSS17a's early-optical and late-NIR emissions in the r -process model, at least two emission regions with different properties are required in the polar or radial direction (Smartt et al. 2017; Waxman et al. 2017). These optical and NIR emissions are called blue and red macronovae, respectively. In the r -process model, since the luminosity is proportional to the ejecta mass, we can estimate the ejecta mass from the observed bolometric luminosity. The detailed light curve or spectral modeling also gives the ejecta mass as $M_{\text{ej}}^{\text{blue}} \simeq 0.02 M_{\odot}$ (Arcavi et al. 2017; Chornock et al. 2017; Cowperthwaite et al. 2017; Drout et al. 2017; Kasen et al. 2017; Kilpatrick et al. 2017; McCully et al. 2017; Nicholl et al. 2017; Smartt et al.

matsumoto@tap.scphys.kyoto-u.ac.jp

¹ Department of Physics, Graduate School of Science, Kyoto University, Kyoto 606-8502, Japan² Center for Gravitational Physics, Yukawa Institute for Theoretical Physics, Kyoto University, Kyoto 606-8502, Japan³ Department of Physics and Mathematics, Aoyama Gakuin University, Sagamihara, Kanagawa, 252-5258, Japan⁴ JSPS Research Fellow⁵ The Raymond and Beverly Sackler School of Physics and Astronomy, Tel Aviv University, Tel Aviv 69978, Israel

2017) and $M_{\text{ej}}^{\text{red}} \simeq 0.03 M_{\odot}$ (Chornock et al. 2017; Cowperthwaite et al. 2017; Drout et al. 2017; Kasen et al. 2017; Kilpatrick et al. 2017; Tanaka et al. 2017b; Utsumi et al. 2017) for the blue and red macronovae, respectively. Given the ejecta masses, the different timescales of the blue (\sim day) and red (\sim 7 days) macronovae suggest different opacities of $\kappa \sim 0.1 - 1 \text{ cm}^2 \text{ g}^{-1}$ and $\kappa \sim 1 - 10 \text{ cm}^2 \text{ g}^{-1}$, respectively. The difference of the opacities reflects the different abundances of the synthesized r -process elements (in particular, lanthanoids in this model, Kasen et al. 2013; Tanaka & Hotokezaka 2013; Tanaka et al. 2017). Numerical simulations of binary NS mergers and nucleosynthesis also suggest some distribution of the ejecta properties (Metzger & Fernández 2014; Perego et al. 2014; Lippuner et al. 2017; Shibata et al. 2017b).

Although the r -process model is broadly accepted as the standard model, it may contain some uncomfortable tensions;

1. First, the total ejecta mass required by the r -process model, $M_{\text{ej}} = M_{\text{ej}}^{\text{blue}} + M_{\text{ej}}^{\text{red}} \simeq 0.05 M_{\odot}$, seems to be relatively larger than that expected by some numerical calculations. Currently, the binary merger calculations show the ejecta mass at the onset of a merger (the dynamical ejecta) $M_{\text{ej}} \lesssim 0.01 - 0.02 M_{\odot}$ (Hotokezaka et al. 2013; Sekiguchi et al. 2015, 2016), except for ones with extremely large mass ratios of $q < 0.7$ (Dietrich et al. 2017), which are not observed in the Galactic binary pulsars (Tauris et al. 2017). The post-merger ejecta such as the viscously-driven outflow may contain rather larger mass of $\gtrsim 0.01 M_{\odot}$ (Fujibayashi et al. 2017b; Shibata et al. 2017b), but its velocity ($v \simeq 0.05 - 0.15 c$, where c is the speed of light) does not seem so large as that suggested by the observations ($v \simeq 0.3 c$, in particular, for the blue macronova). We also remark that the exact values may depend on the prescription of the neutrino transfer and the viscosity. Intriguingly, massive ejecta were also suggested by the macronova candidates accompanying GRBs 050709, 060614, and 130603B ($\sim 0.03 - 0.1 M_{\odot}$, Berger et al. 2013; Tanvir et al. 2013; Yang et al. 2015; Jin et al. 2016).
2. Given the merger rate estimated from this event, the necessary ejecta mass in the r -process model could result in a larger production rate of the r -process elements than that suggested by the solar abundance (see also Cowperthwaite et al. 2017). Combining the observed NS merger rate of $\mathcal{R} \simeq 1540_{-1220}^{+3220} \text{ Gpc}^{-3} \text{ yr}^{-1}$ (Abbott et al. 2017) with the estimated ejecta mass of $M_{\text{ej}} \simeq 0.05 M_{\odot}$ gives the r -process production rate in a galaxy of $\dot{M}_r = \mathcal{R} M_{\text{ej}} / n_{\text{Gal}} \simeq 7.7_{-6.1}^{+16.1} \times 10^{-6} M_{\odot} \text{ yr}^{-1}$, where we use the number density of galaxies of $n_{\text{Gal}} \simeq 0.01 \text{ Mpc}^{-3}$. The central value of the above production rate is ten times larger than the Galactic production rate of $\simeq 7 \times 10^{-7} M_{\odot} \text{ yr}^{-1}$ for the r -process elements with mass numbers $A \gtrsim 100$ (Qian 2000). Of course, we should remark again that the adopted merger rate is determined only by GW170817.

3. It is also uncertain whether the ejecta required to explain SSS17a can reproduce the Galactic r -process abundance pattern or not. In order to explain the solar abundance pattern, the lanthanoid mass fraction of $X_{\text{Lan}} \sim 10^{-1.5}$ is required for the ejecta composed of r -process elements. However, for instance, Waxman et al. (2017) conclude that the observation of SSS17a suggests the ejecta's lanthanoid mass fraction of $X_{\text{Lan}} \sim 10^{-3}$.
4. Compared with the other sGRBs, the light curve of SSS17a suggests that there may be a diversity in the macronova luminosity (Fong et al. 2017; Gompertz et al. 2017). The luminosity dispersion could have a range of two-orders of magnitudes. In the r -process model, if the previous macronovae were also produced by binary NSs and had similar spectra to this event, the dispersion of the luminosity reflects the diversity of the ejecta mass. However, such a broad diversity in ejecta mass may not be produced in particular by the dynamical coalescence phase, which depends on the binary's total mass and mass ratio showing narrow distributions among the Galactic binary pulsars (Tauris et al. 2017). The post-merger ejecta such as the viscously-driven outflow may explain the diversity due to the differences of the magnetic fields or the collapse time of remnant hypermassive NSs to black holes (BHs), but the numerical calculations are not conclusive yet.
5. The gamma-, X-ray, and radio observations suggest the existence of energetic ejecta such as a relativistic jet or a mildly-relativistic cocoon (LIGO Scientific Collaboration, et al. 2017b; Alexander et al. 2017; Evans et al. 2017; Fong et al. 2017; Goldstein et al. 2017; Haggard et al. 2017; Hallinan et al. 2017; Ioka & Nakamura 2017; Kasliwal et al. 2017; Margutti et al. 2017; Murguia-Berthier et al. 2017; Savchenko et al. 2017; Troja et al. 2017). These ejecta can easily inject energy into the macronova components and affect the emissions.

Then, it is worth considering another energy source rather than the radioactive heating by the r -process elements, and discussing whether the energy source can explain the observation or not. In this work, we consider the energy injection from the central engine activities as the energy source, and call this model as the *engine model*. Different from the r -process model, the energy source is decoupled with the ejecta mass, so that wider ranges of the ejecta mass and opacity are allowed in the engine model. In particular, the engine model can reproduce the macronova by less ejecta mass than that needed by the r -process model, and may resolve the above concerns 1 and 2. Furthermore, since the jet activities actually show the diversity in the luminosity or energy, the diversity of macronovae (concern 4) can be also explained by the difference of the injection energy.

So far, the energy injection mechanisms have been discussed and applied to the macronova in GRB 130603B (Kisaka et al. 2015, 2016). Some sGRBs show long-lasting jet activities such as the extended emissions ($\sim 10^2 \text{ s}$, Barthelmy et al. 2005) and the plateau emissions

($\sim 10^{4-5}$ s, Gompertz et al. 2013, 2014), which may result from the activities of the central engine (Ioka et al. 2005). If a rapidly rotating magnetar is formed as the central engine, its large spin-down energy can produce a bright (or even brighter) optical emission like a macronova (Yu et al. 2013; Metzger & Piro 2014). Since a long-lived magnetar makes the emission too bright, the magnetar likely collapses to a BH in a short timescale. After the collapse, the BH launches a jet and injects energy into the ejecta by radiations or shocks, reproducing the macronova (Kisaka et al. 2015). In addition, a mysterious X-ray excess with comparable duration ($\simeq 7$ days) and luminosity ($\simeq 10^{41-42}$ erg s $^{-1}$) was also detected in GRB 130603B (Fong et al. 2014). If the X-ray excess was emitted quasi-isotropically and absorbed by the ejecta, the reprocessed emission of the X-rays is also able to produce the macronova emission (Kisaka et al. 2016). For SSS17a, Ioka & Nakamura (2017) show that the blue macronova could be powered by the prompt jet only (see also, Piro & Kollmeier 2017). Yu & Dai (2017) also discuss the energy injection from the spin-down of a remnant hypermassive NS, although the NS should keep unrealistically small magnetic fields $B \sim 10^{11-12}$ G.

The observations of SSS17a supply very rich data in contrast to GRB 130603B with only one-epoch detection and other macronova candidates. In this work, we extend the engine model and test whether the energy injection can explain the extensively observed macronova, SSS17a or not. The structure of this paper is as follows. In section 2, we discuss the basic concept of our engine model and show that this model can reproduce the observed macronova with order-of-magnitude estimations. The engine model allows a large parameter space to explain this event. We argue that some parameter sets are actually motivated from numerical simulations. Then, in section 3, we construct simple light curve models and show that the models agree with the observation, with smaller ejecta mass than that required in the r -process model, and with the observationally-motivated energy injection channel. Finally we discuss the implications of our study and the prospect of the future observations in section 4.

2. ENGINE MODEL

The observed macronova showed a transition from the optical (~ 1 day) to the NIR emissions (~ 1 week). We call the early-optical and late-NIR emissions as blue and red macronovae, respectively. We estimate the emission radii of the blue and red macronovae by using the observables (Drout et al. 2017; Kasliwal et al. 2017; Kilpatrick et al. 2017). Let us consider an ejecta emitting photons and subtending a fraction Ω of the solid angle. By assuming blackbody radiation, the emission radius with the luminosity L and temperature T is given by

$$R = \sqrt{\frac{L}{4\pi\Omega\sigma T^4}}, \quad (1)$$

where σ is the Stefan-Boltzmann constant. With the observables, the emission radii of the blue and red macrono-

vae are estimated by

$$R_{\text{blue}} \simeq 9.0 \times 10^{14} \text{ cm} \left(\frac{T}{7000 \text{ K}} \right)^{-2} \left(\frac{L}{7 \times 10^{41} \text{ erg s}^{-1}} \right)^{1/2} \Omega_{0.5}^{-1/2}, \quad (2)$$

$$R_{\text{red}} \simeq 1.7 \times 10^{15} \text{ cm} \left(\frac{T}{3000 \text{ K}} \right)^{-2} \left(\frac{L}{8 \times 10^{40} \text{ erg s}^{-1}} \right)^{1/2} \Omega_{0.5}^{-1/2}, \quad (3)$$

where we use $\Omega = 0.5\Omega_{0.5}$. By dividing each radius by each timescale, we infer the expanding velocities of $v_{\text{blue}} \simeq 0.3c$ and $v_{\text{red}} \simeq 0.1c$, respectively, where c is the speed of light. Note that after 7 days, the red macronova is no longer approximated by a blackbody spectrum (Chornock et al. 2017; Kilpatrick et al. 2017; Nicholl et al. 2017; Pian et al. 2017; Shappee et al. 2017). The difference of the photospheric velocities suggests that the blue and red macronovae are powered by the different emission regions along the polar or radial direction.

The large range of the emission timescale from 1 day to 7 days suggests that there are at least two emission regions contained by more than one component of ejecta. It should be noted that the two emission regions are not necessarily contained by two ejecta components separately. For example, the observed light curve of the macronova is well fitted by a single-component-ejecta models (see Smartt et al. 2017; Waxman et al. 2017). Before discussing our model, we define the meaning of the word “component” of ejecta. In the following, we discuss the properties of various ejecta. When we can specify an ejecta based on its physical origin such as the dynamical ejecta or post-merger ejecta (see below), we call each ejecta as “component”. These components have some continuous opacity, density, and velocity distributions, which produce emission regions with different properties such as emission timescales.

In the engine model, emissions are not powered by the radioactive decay of r -process elements, but by the activity of the central engine, which allows large parameter spaces of the ejecta mass and opacity. In order to see this, we first consider that the injected energy is released by the photon diffusion, so-called the cooling emission. The characteristic timescale of the cooling emission is set by the condition of $\tau = c/v$, where τ and v are the optical depth and velocity of the ejecta, respectively.⁶ The diffusion time of the ejecta with an opacity κ and mass M is given by (Arnett 1980)

$$t_{\text{diff}} \simeq \sqrt{\frac{\xi\kappa M}{\Omega v c}}, \quad (4)$$

where ξ is a numerical factor reflecting the density structure of the ejecta. For instance, Arnett (1980) originally evaluated the factor as $\xi \simeq 2/13.7$, and we use $\xi = 3/4\pi \simeq 0.24$ in the one-zone model and $\xi \simeq 0.026$ for ejecta with a power-law density distribution (see section

⁶ The diffusion timescale also gives the peak timescale of the emission in the r -process model.

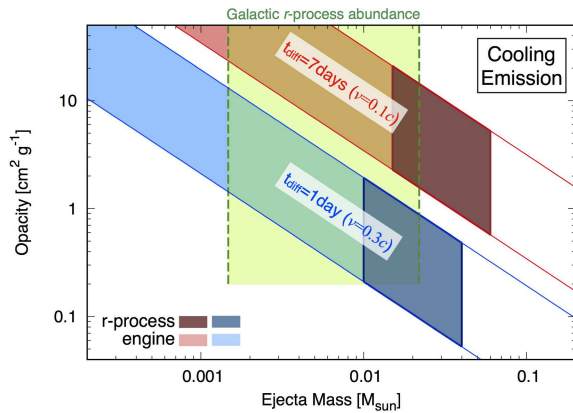


FIG. 1.— The required ejecta mass and opacity regions to reproduce the observed blue ($t_{\text{diff}} \simeq 1$ day) and red ($t_{\text{diff}} \simeq 7$ days) macronovae with cooling emissions in the engine model. The dark-red and dark-blue regions denote the mass and opacity suggested in the r -process model. The green shaded region shows the required total ejecta mass to explain the Galactic r -process abundance with the event rate estimated by GW170817. The engine model allows much larger parameter ranges than the r -process model.

3). The observed macronova showed a large timescale range of 1 – 7 days which may be difficult to reproduce by a single combination of the opacity and mass. Then, we consider at least two components of ejecta with different values of the product κM or a single component with a polar or radial distribution of κM . By using the emission timescales of 1 and 7 days, and the ejecta velocities of $v_{\text{blue}} = 0.3c$ and $v_{\text{red}} = 0.1c$, the products are constrained as

$$\kappa M \simeq 2.1 \times 10^{-3} \text{ cm}^2 \text{ g}^{-1} M_{\odot} \left(\frac{v_{\text{blue}}}{0.3c} \right) \left(\frac{t_{\text{diff}}}{1 \text{ day}} \right)^2 \left(\frac{\xi}{3/4\pi} \right)^{-1} \Omega_{0.5}, \quad (5)$$

$$\kappa M \simeq 3.4 \times 10^{-2} \text{ cm}^2 \text{ g}^{-1} M_{\odot} \left(\frac{v_{\text{red}}}{0.1c} \right) \left(\frac{t_{\text{diff}}}{7 \text{ day}} \right)^2 \left(\frac{\xi}{3/4\pi} \right)^{-1} \Omega_{0.5}, \quad (6)$$

for the blue and red macronovae, respectively. In Fig. 1, we show the constraints on the ejecta mass and opacity imposed by the observed timescales. The red and blue shaded regions show the above constraints on κM taking the uncertainty of the coefficient ξ in Eq. (4) into account. The dark-red and dark-blue regions show the parameter spaces in the r -process model. In order to explain the observations in the engine model, the mass should be smaller than that required in the r -process model. The green shaded region denotes the total ejecta mass required to explain the Galactic r -process abundance with mass numbers $A \gtrsim 100$ by only binary NS mergers with the event rate estimated by this event, $\mathcal{R} \simeq 1540_{-1220}^{+3220} \text{ Gpc}^{-3} \text{ yr}^{-1}$ (Abbott et al. 2017). Since the low opacity value of $\sim 0.2 \text{ cm}^2 \text{ g}^{-1}$ is realized by hydrogen or iron without r -process elements, the green shaded region has a boundary at the low opacity. In principle, the ejecta in the blue and red shaded regions can reproduce the observed blue and red macronovae, respectively, in the engine model.

2.1. Ejecta

In the following, we discuss possible ejecta components, which are motivated by the recent numerical simulations, although the engine model allows more general configurations as in Fig. 1.

2.1.1. Merger Ejecta

One is the *merger ejecta*. The merger ejecta includes the dynamical ejecta (Hotokezaka et al. 2013; Sekiguchi et al. 2015, 2016) and the post-merger ejecta such as the neutrino-driven winds (Dessart et al. 2009; Wanajo & Janka 2012; Perego et al. 2014; Fujibayashi et al. 2017) and more importantly viscously-driven outflows (Fernández & Metzger 2013; Fernández et al. 2015a,b; Kiuchi et al. 2014, 2015; Giacomazzo et al. 2015; Ciolfi et al. 2017; Shibata et al. 2017; Siegel & Metzger 2017; Fujibayashi et al. 2017b). For example, we can consider the following set of parameters: $\kappa_e = 10 \text{ cm}^2 \text{ g}^{-1}$, $M_e = 10^{-2} M_{\odot}$, and $v_e = 0.1c$. It should be noted that as long as the product of κ_e and M_e has the same value, the resulting emission has a similar signature in the engine model.

The dynamical ejecta is produced by the shock heating and the tidal interaction at the onset of the merger. The ejecta mass and velocity depend on the equation of state of nuclear matter, the binary mass ratio, and so on. Numerical relativity simulations show typical values of $M_e \sim 10^{-3} - 10^{-2} M_{\odot}$ and $v_e \simeq 0.1 - 0.2c$.⁷ The dynamical ejecta may have different opacities depending on the angular direction (Wanajo et al. 2014; Tanaka et al. 2017). In the equatorial direction, the ejecta is launched mainly by the tidal force and has a low electron fraction of $Y_e \sim 0.1 - 0.2$ due to the inefficient heating. In such a very neutron rich ejecta, the nucleosynthesis advances up to the third peak and produces lanthanoid elements, which results in the opacity as high as $\kappa_e \sim 10 \text{ cm}^2 \text{ g}^{-1}$. On the other hand, shock heating also drives ejecta quasi-spherically and raises its electron fraction $Y_e \gtrsim 0.25$. Then, the shock-heated dynamical ejecta has rather small opacity of $\kappa_e \sim 0.1 - 1 \text{ cm}^2 \text{ g}^{-1}$ (Sekiguchi et al. 2015, 2016; Wanajo et al. 2014; Tanaka et al. 2017). In this case, the opacity smoothly increases from the polar to the equatorial direction.

The post-merger ejecta is launched by the merger remnant object and the accretion disk into the polar direction. The ejecta is less neutron rich and has a small opacity $\kappa_e \sim 0.1 - 1 \text{ cm}^2 \text{ g}^{-1}$. The typical velocity and mass are $v_e \simeq 0.05c - 0.15c$ and $M_e \sim 10^{-2} M_{\odot}$ (Siegel & Metzger 2017; Fujibayashi et al. 2017b; Shibata et al. 2017b), but these values depend on the neutrino transport and the viscosity prescription in numerical simulations. The post-merger ejecta is located in the inner region of the dynamical ejecta because its velocity is smaller than that of the dynamical ejecta.

2.1.2. Cocoon

The other is the *cocoon*. When a relativistic jet is launched from the central engine and propagates in the merger ejecta on the polar axis, the jet energy is dissipated and injected into the cocoon. The

⁷ We do not consider the ultra-relativistic ejecta from the shock breakout of NSs (Kyutoku et al. 2014).

duration of the engine activity determines whether the prompt jet successfully breaks out of the merger ejecta or not. Now successful and choked jet scenarios are proposed in order to explain the prompt gamma-ray emission and the radio and X-ray afterglows associated with GW170817 (Kasliwal et al. 2017; Gottlieb et al. 2017b; Ioka & Nakamura 2017; Lazzati et al. 2017; Mooley et al. 2017; Margutti et al. 2018; Nakar & Piran 2018). In this event, both models predict the cocoon with similar properties such as the mass and velocity. When the jet drills through the merger ejecta successfully, the cocoon also breaks out of the ejecta and expands isotropically.⁸ Even when the jet is choked within the merger ejecta, if a sufficient energy is injected into the cocoon, it breaks out of the ejecta (Gottlieb et al. 2017b).

The cocoon parameters are evaluated as follows. The dissipated jet energy is evaluated by $E_{\text{jet}} \sim L_j t_j = 5 \times 10^{50} \text{ erg} (L_j / 5 \times 10^{50} \text{ erg s}^{-1})(t_j / 1 \text{ s})$, where L_j and t_j is the geometrically-corrected jet luminosity and the duration of the prompt-jet launching time, respectively. The cocoon mass is determined by the volume swept by the cocoon's shock. In the case of short GRB jets, differently from long GRB jets, the cocoon mass is evaluated by $M_c \sim 5 \times 10^{-3} M_\odot (M_e / 0.01 M_\odot)(\theta_j / 0.3)$, where M_e and θ_j are the merger ejecta's mass and the jet opening angle, respectively (Ioka & Nakamura 2017). The adopted jet opening angle $\theta_j = 0.3 \text{ rad} \simeq 17^\circ$ is consistent with the mean angle suggested by the observations ($\theta_j \simeq 16^\circ \pm 10^\circ$, Fong et al. 2015), which could also explain the observations of sGRB 170817A, blue macronova, X-ray and radio-afterglows following GW170817 for the successful jet breakout (Ioka & Nakamura 2017). Then, the velocity is given by $v_c \sim \sqrt{2E_{\text{jet}}/M_c} \sim 0.3c (E_{\text{jet}}/5 \times 10^{50} \text{ erg})^{1/2} (M_c/5 \times 10^{-3} M_\odot)^{-1/2}$. The cocoon has likely rather small opacity of $\kappa_c \simeq 0.5 \text{ cm}^2 \text{ g}^{-1}$, because it is made of the polar directed merger ejecta, which is dominated by high electron fraction ejecta of $Y_e > 0.25$ and synthesizes less opaque elements (Sekiguchi et al. 2015, 2016; Wanajo et al. 2014; Tanaka et al. 2017, and see also section 2.1.1). It should be noted again that only the product $\kappa_c M_c$ is important to reproduce the light curve in the engine model.

2.2. Energy Sources

We consider an alternative to r -process radioactivity for the energy source of the blue and red macronovae: the central engine activities. We discuss two kinds of observationally-motivated energy sources from the engine activities and evaluate the emission timescales of the ejecta.

2.2.1. Jets

A jet launched by the central engine can inject energy into ejecta in the polar direction by high energy radiations or shocks. Since a cocoon is formed near the polar axis, we consider that the cocoon is heated up by the energy injection from the jet activities and powers a cooling emission.

⁸ We mainly focus on the dominant, sub-relativistic cocoon, not on the mildly-relativistic cocoon (Nakar & Piran 2017; Gottlieb et al. 2017).

In addition to the prompt emissions, some sGRBs show extended and plateau emissions (Kisaka et al. 2015, 2017; Ioka & Nakamura 2017), which may result from the long-lasting jet activities. These emissions are too dim to be detected by an off-axis observer in this event. Recently, Kisaka et al. (2017) investigated 65 sGRBs' X-ray light curves in *Swift*/BAT and XRT data, and found that the typical (geometrically-corrected)⁹ injection energy and time are $E_{\text{in}}(\sim E_{\text{jet}}) \sim 10^{48-51} \text{ erg}$ and $t_{\text{in}} \sim 10^2 \text{ s}$ for the extended emissions, and $E_{\text{in}} \sim 10^{47-51} \text{ erg}$ and $t_{\text{in}} \sim 10^{4-5} \text{ s}$ for the plateau emissions, respectively. Since the injection energy is less than that injected by the prompt jet, the cocoon is not accelerated any more.

Due to the heating, the jet-powered cocoon radiates photons for a day. The characteristic photon diffusion timescale is given by Eq. (4),

$$t_{\text{diff}} \simeq 1.1 \text{ day } \kappa_c^{1/2} M_c^{1/2} v_{c,0.005}^{-1/2} \Omega_{0.5}^{-1/2} \left(\frac{\xi}{3/4\pi} \right)^{1/2}, \quad (7)$$

where we use $\kappa_c = 0.5 \kappa_{c,0.5} \text{ cm}^2 \text{ g}^{-1}$, $M_c = 5 \times 10^{-3} M_{c,0.005} M_\odot$, and $v_c = 0.3 c v_{c,0.3}$. We define the fraction of the solid angle subtended by the jet-powered ejecta as $\Omega = 1 - \cos \theta$, where θ is the half apex angle of the ejecta (see Fig. 3). We consider the cocoon in a one-zone model (see below Eq. (4) for the fiducial values of ξ). The luminosity at $t = t_{\text{diff}}$ is estimated by dividing the internal energy by the diffusion time, $L \simeq E_{\text{int}}(t = t_{\text{diff}})/t_{\text{diff}}$. Until the photons start to diffuse out, the internal energy suffers from the adiabatic cooling and decreases as $E_{\text{int}}(t) = E_{\text{in}}(t/t_{\text{in}})^{-1}$. Then, the diffusion luminosity is given by $L \sim E_{\text{in}} t_{\text{in}} / t_{\text{diff}}^2$. Therefore, by the energy injection of $E_{\text{in}} t_{\text{in}} \sim 7 \times 10^{51} \text{ erg s}$, the diffusion luminosity reaches $L \sim 10^{42} \text{ erg s}^{-1}$ at $t_{\text{diff}} \sim 1 \text{ day}$ in optical bands. Finally, we remark that a similar energy injection scenario is discussed in Kasliwal et al. (2017) (see their supplementary material), where the engine-driven wind injects energy into the ejecta.

2.2.2. Long-Lasting X-ray Luminosity

We may have another energy source, which is motivated by the X-ray observation of GRB 130603B. This event showed a mysterious X-ray excess with a long duration of $\sim 7 \text{ days}$, and a luminosity larger than the extrapolation from its afterglow and showing a power-law temporal decaying of $L_X(t) \propto t^{-\alpha_X}$ (Fong et al. 2014), where α_X is the temporal index. Such an X-ray excess could be produced by the fallback accretion onto the central engine (Rosswog 2007; Rossi & Begelman 2009; Kisaka & Ioka 2015). More interestingly, the excess X-ray luminosity is comparable with the luminosity of the NIR macronova associated with GRB 130603B. If the X-ray excess emission is quasi-isotropic and absorbed by the merger ejecta, the reprocessed NIR photons can reproduce the NIR macronova without introducing any other energy sources such as the radioactive energy (Kisaka et al. 2016).

We consider that the cocoon and merger ejecta are irradiated by the long-lasting X-ray emission, which is

⁹ Kisaka et al. (2017) studies the isotropic radiated energy $E_{\text{iso,rad}}$, and the injection energy is evaluated by $E_{\text{in}} \sim E_{\text{jet}} \sim (\theta_j/0.3)^2 (\eta/0.1)^{-1} E_{\text{iso,rad}}$, where η is the emission efficiency.

similar to the mysterious X-ray excess observed in GRB 130603B. Then, the ejecta produce optical and NIR emissions for $\sim 1 - 7$ days by reprocessing X-rays, which are observed as the macronova. Note that when jet activities inject less energy than the X-ray excess, the reprocessed emission dominates the cocoon emission. Even without the cocoon, the irradiated merger ejecta may also produce the blue macronova of ~ 1 day, if some part of the ejecta has small κM (see below). For instance, the opacity of the merger ejecta may distribute from a large value ($\kappa \sim 10 \text{ cm}^2 \text{ g}^{-1}$) at the equatorial plane to a low value ($\kappa \sim 0.1 - 1 \text{ cm}^2 \text{ g}^{-1}$) at the polar axis (see also section 2.1.1). A distribution of κM is also realized even with a constant opacity for the whole ejecta, when the ejecta mass is distributed along the polar or radial direction. In principle, the central engine activity can last for a long time of ~ 7 days and isotropically irradiate the ejecta by X-rays with the luminosity of $L_X \sim 10^{41-42} \text{ erg s}^{-1}$ (Fong et al. 2014, 2016; Kisaka et al. 2017). Because the bound-free opacity of X-rays is much larger than that of optical and NIR photons, the ejecta absorb the X-rays and reprocess them into lower energy photons. We do not observe the X-ray excess in this event, because we see GW170817 from off-axis angle as suggested by the prompt emission and afterglow observations, and the X-rays are absorbed by the merger ejecta.

For the reprocessed photons to escape from the ejecta, the ejecta should be “diffusively thin”. Moreover, for the diffusing photons to show a blackbody spectrum, the ejecta should also be “optically thick”. It should be noted that these two conditions are defined by different two concepts. When the diffusion time of the ejecta is shorter than the dynamical timescale, photons can diffuse out of the ejecta after multiple scatterings. This situation is called as diffusively thin, and expressed as

$$t > t_{\text{diff}} \simeq 4.0 \text{ day } \kappa_{e,10}^{1/2} M_{e,0.01}^{1/2} v_{e,0.1}^{-1/2} \Omega_{0.5}^{-1/2} \left(\frac{\xi}{0.026} \right)^{1/2} \quad (8)$$

where we normalize ξ with 0.026 by taking the density structure into account (see section 3). We use $\kappa_e = 10 \kappa_{e,10} \text{ cm}^2 \text{ g}^{-1}$, $M_e = 10^{-2} M_{e,0.01} M_\odot$, and $v_e = 0.1 c v_{e,0.1}$. The diffusion time of the cocoon is given in Eq. (7). In the optically thick ejecta, the photons are scattered and thermalized. The timescale when the ejecta becomes optically thin is evaluated by equating the optical depth with unity. Then, the condition that the ejecta is optically thick is written as

$$t < t_{\text{tr}} \simeq \sqrt{\frac{\xi \kappa M}{\Omega v^2}} = t_{\text{diff}} \left(\frac{c}{v} \right)^{1/2}, \quad (9)$$

$$\simeq 12.4 \text{ day } \kappa_{e,10}^{1/2} M_{e,0.01}^{1/2} v_{e,0.1}^{-1} \Omega_{0.5}^{-1/2} \left(\frac{\xi}{0.026} \right)^{1/2} \quad (10)$$

$$\simeq 2.0 \text{ day } \kappa_{c,0.5}^{1/2} M_{c,0.005}^{1/2} v_{c,0.3}^{-1} \Omega_{0.5}^{-1/2} \left(\frac{\xi}{3/4\pi} \right)^{1/2} \quad (11)$$

The second and third lines correspond to the timescales of the merger ejecta (with a density distribution) and the cocoon (in the one-zone approximation), respectively. As long as $t_{\text{diff}} < t < t_{\text{tr}}$, the reprocessed luminosity is $L \sim L_X$. If the ejecta is otherwise diffusively thick ($t < t_{\text{diff}}$), the reprocessed photons are trapped in the ejecta and

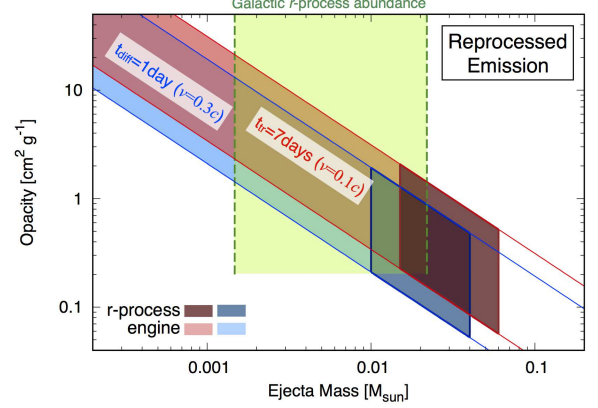


FIG. 2.— The same as for Fig. 1 but for the reprocessed emissions in the engine model.

suffer from adiabatic cooling. If the ejecta is optically thin ($t > t_{\text{tr}}$) instead, the reprocessed photons may not thermalize from X-ray to optical and NIR emissions. We also remark that we use the grey opacity to estimate the optical depth for simplicity while the realistic opacity depends on wavelengths.

Since the reprocessed emission with a blackbody spectrum continues for $t_{\text{diff}} < t < t_{\text{tr}}$, we can constrain these timescales by observations. When the blue macronova is produced by the reprocessed emission, its short timescale $\lesssim 1$ day gives an upper limit on the diffusion timescale, which results in a limit on κM . In Fig. 2, we show this constraint with a blue shaded region. This region is basically the same as the region in Fig. 1 and Eq. (5). On the other hand, since the red macronova showed spectra deviating from a blackbody at later time ($\gtrsim 7$ days, Chornock et al. 2017; Kilpatrick et al. 2017; Nicholl et al. 2017; Pian et al. 2017; Shappee et al. 2017), these observations constraint the optically-thin timescale as $t_{\text{tr}} \simeq 7$ days, which results in a constraint on κM as

$$\kappa_e M_e \simeq 3.2 \times 10^{-2} \text{ cm}^2 \text{ g}^{-1} M_\odot \left(\frac{v_{\text{red}}}{0.1 c} \right)^2 \left(\frac{t_{\text{tr}}}{7 \text{ day}} \right)^2 \left(\frac{\xi}{0.026} \right)^{-1} \Omega_{0.5}. \quad (12)$$

We show this condition in Fig. 2 as a red shaded region. When the ejecta satisfying this condition are irradiated by an X-ray excess, the reprocessed emission can explain the red macronova with $t_{\text{tr}} \simeq 7$ days. Interestingly, both of the blue and red macronovae can be produced by the ejecta with a single combination of κM in the reprocessed emission model (but different velocities are required).

Note that the same condition (Eq. (12)) should be imposed on the ejecta in the r -process model. Waxman et al. (2017) construct a light curve model taking the optically-thin timescale into account. In particular, our results are consistent with their conclusions.

3. LIGHT CURVE MODELS

Based on the order-of-magnitude estimation in the last section, we consider possible combinations of ejecta and energy injections, and construct simple light curve models in this section. We show that the engine model can

TABLE 1
POSSIBLE COMBINATIONS OF EJECTA AND ENERGY INJECTIONS

Blue Macronova		Red Macronova	
ejecta ($\kappa M \sim 10^{-3}$)	energy source	ejecta ($\kappa M \sim 10^{-2}$)	energy source
(A) cocoon	jet	merger ejecta(eq)	X-ray
(B) cocoon	X-ray	merger ejecta(eq)	X-ray
(C) merger ejecta(po)	X-ray	merger ejecta(eq)	X-ray
(D) merger ejecta(eq)	X-ray	merger ejecta(po)	X-ray

Notes. The values of κM are written in a unit of $\text{cm}^2 \text{g}^{-1} M_\odot$. The location (polar and equatorial directions) of the merger ejecta is represented by “po” and “eq”, respectively.

reproduce the observed macronova with various configurations.

In Table 1, we list the possible combinations of ejecta and energy sources to reproduce the macronova. Since the engine model allows the large parameter space (see Figs. 1 and 2), various combinations are possible. When we consider two component ejecta such as the cocoon and the merger ejecta, we have two situations depending on their energy sources. In these models, we consider the merger ejecta in the equatorial direction, which have the large opacity and produce a long emission timescale. In model (A), the cocoon and the merger ejecta are separately powered by the jet activity and X-ray excess emission. Then, the diffusion emission from the cocoon and the reprocessed emission from the merger ejecta produce the blue and red macronovae, respectively. In Fig. 3, we show schematic pictures of this model. As we discuss in section 2.1.2, regardless of the successful and choked jets (left and right panels of Fig. 3), the cocoon may break out of the merger ejecta. In model (B), both cocoon and merger ejecta are powered by the X-ray excess and produce the blue and red macronovae, respectively. In this model, we assume that the jet activity is not so powerful to power the cocoon.

We can also consider the cases where both blue and red macronovae are produced by the merger ejecta. Since the merger ejecta (dynamical ejecta) have the directional opacity distribution, the polar and equatorial directed ejecta may produce the blue and red macronovae, respectively, if they are irradiated by the X-ray excess. Even with a constant opacity, if the ejecta mass has a polar distribution, the polar ejecta with a small mass and the equatorial ejecta with a large mass can produce the blue and red macronovae, respectively. We name these situations as model (C). As another possibility, when the post-merger ejecta (polar directed) have larger mass and hence larger κM than the dynamical ejecta (equatorial directed), the merger ejecta in the polar and equatorial directions may produce the red and blue macronovae, respectively, irradiated by the X-ray luminosity (model (D)).

In the reprocessed emission model, we do not consider the configuration where a single component ejecta has a radial κM distribution, because such profile can not reproduce the emission timescales. Since X-rays are absorbed at the inner part of the ejecta due to a large κM , the reprocessed photons can not leak out from this inner part in the observed short timescale.

In the following subsections, we construct simple light curve models focusing on models (A) and (B). The same procedure is applied to the other models and gives similar

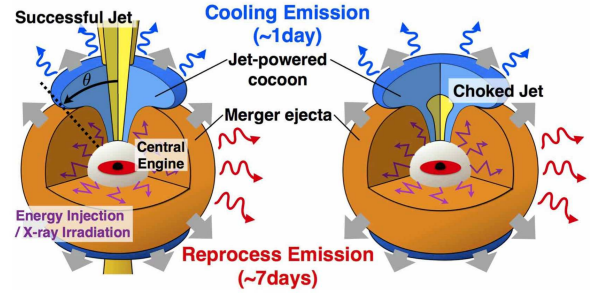


FIG. 3.— The schematic picture of the jet-powered cocoon and the merger ejecta, which are powered by the jet activities and the quasi-isotropic X-ray excess, respectively. Left and right figures show the cases of the successful and the choked jets. These figures correspond to model (A) in Table 1.

light curves.

3.1. Cooling Emission from Jet-Powered Cocoons

First, we consider the light curve of the cooling emission from the jet-powered cocoon, which produces the blue macronova in model (A). We construct a simple emission model by a one-zone approach. The jet-powered cocoon with mass M_c and velocity v_c expands homologously into a fraction Ω of the solid angle. The outermost radius of the ejecta is given by $R = v_c t$, which coincides with the photosphere for the early phase of $t \lesssim t_{\text{diff}} (< t_{\text{tr}})$. The time evolution of the diffusion luminosity is simply given by considering the thermodynamics of the ejecta (Arnett 1980; Matsumoto et al. 2016). The first law of thermodynamics is given by

$$\frac{dE}{dt} = -P \frac{dV}{dt} - L + H, \quad (13)$$

where E , P , $V = 4\pi\Omega R^3/3$, L , and H is the total internal energy, pressure, volume, diffusion luminosity, and heating from the radioactive decay. The pressure is dominated by the radiation $P = E/3V$. The diffusion luminosity is evaluated by the diffusion approximation as $L \simeq tE/t_{\text{diff}}^2$. We neglect the radioactive decay heating, which is justified as long as the cocoon mass is smaller than that required in the r -process model ($\simeq 0.02 M_\odot$, see Fig. 1). With the initial condition of $E = E_{\text{in}}$ at $t = t_{\text{in}}$, we can easily integrate Eq. (13) and obtain the time evolution of the internal energy and the luminosity as

$$L(t) = \frac{E_{\text{in}} t_{\text{in}}}{t_{\text{diff}}^2} \exp\left(-\frac{t^2 - t_{\text{in}}^2}{2t_{\text{diff}}^2}\right). \quad (14)$$

The observed photospheric temperature is given by using the photospheric radius $R_{\text{ph}} \sim v_c t$ and the bolometric luminosity as

$$T_{\text{ph}} = \left(\frac{L}{4\pi\Omega R_{\text{ph}}^2 \sigma}\right)^{1/4}. \quad (15)$$

We also assume the blackbody spectrum to depict light curves (Cowperthwaite et al. 2017; Kilpatrick et al.

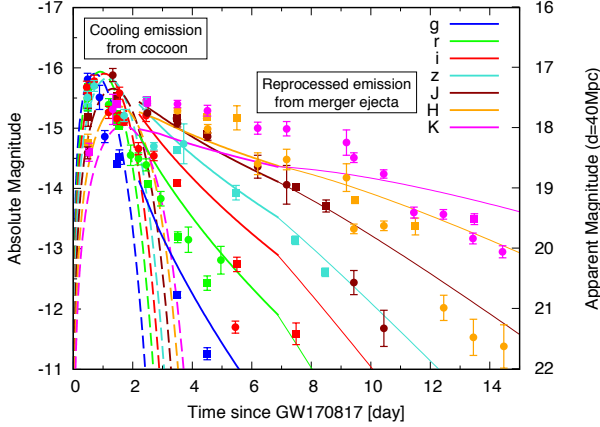


FIG. 4.— The light curves of the diffusion emission from jet-powered cocoon (dashed) and the reprocessed emission from the merger ejecta (solid), respectively (model (A)). For the merger ejecta, we show the light curves in the diffusively thin and optically thick phase $t_{\text{diff}} < t < t_{\text{tr}}$ and optically thin phase $t_{\text{tr}} < t$ with thick and thin solid curves, respectively. Both light curves show good agreements with the observed data points taken from Kasiwal et al. (2017) (circle) and Drout et al. (2017) (square). By the jet activities, the jet-powered cocoon receives the energy which powers the blue macronova. The red macronova is emitted from the merger ejecta as the NIR emission reprocessed from the quasi-isotropic X-ray excess produced by the central engine.

2017; McCully et al. 2017; Nicholl et al. 2017; Shappee et al. 2017; Valenti et al. 2017).

In Fig. 4, the light curves of the jet-powered cocoon show a good agreement with the observed blue macronova. We show the light curves with dashed curves, and the observed data points taken from Kasiwal et al. (2017) and Drout et al. (2017). The parameters of the ejecta and energy injections are listed in Tables 2. The required injection energy (or $E_{\text{in}}t_{\text{in}}$) are supplied by jet activities, such as the prompt, extended, and plateau emissions. The light curves show a rapid decay after $t \gtrsim t_{\text{diff}}$ because the photons diffuse out after the diffusion time.

In Fig. 5, the red and blue dashed curves denote the bolometric luminosity and the photospheric temperature, respectively. We also show the observed bolometric luminosity, which is derived by summing up the flux in each band, and the photospheric temperature, which fits the observed spectra with a blackbody (Kilpatrick et al. 2017). The calculated luminosity and temperature roughly agree with the observed ones.

Piro & Kollmeier (2017) also consider the early-optical emission as the cocoon emission and construct a light curve model based on Nakar & Piran (2017). In contrast to our one-zone approach, they assume an internal structure of the ejecta and calculate the light curve. They mainly focus on the prompt jet as the energy injection channel, while we consider more injection processes such as the extended and plateau emissions.

3.2. Reprocessed Emission

Next, we consider the reprocessed emissions from the merger ejecta (for models (A)-(D)) and the cocoon (for model (B)).

3.2.1. Reprocessed Emission from Merger Ejecta

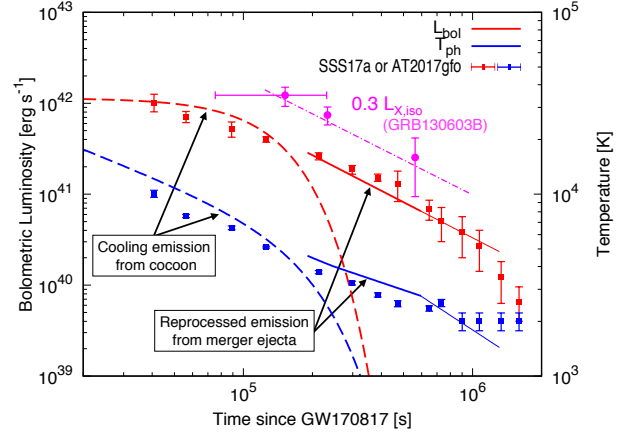


FIG. 5.— The time evolution of bolometric luminosity (red) and photospheric temperature (blue) of the jet-powered cocoon (dashed; blue macronova) and the merger ejecta (solid; red macronova), respectively, in model (A). The red and blue data points denote the observed luminosity and temperature of the red and blue macronovae (SSS17a or AT2017gfo), which are taken from Kilpatrick et al. (2017). The engine model successfully reproduces the observation data. We also show the observed X-ray excess luminosity of GRB 130603B taken from Fong et al. (2014), which has the same slope with the red macronova, $\alpha_X \simeq 1.3$.

We first discuss the emission from the merger ejecta using the formulation in Kisaka et al. (2015), and later apply the same formalism to the cocoon. Since the energy injection from the central engine is not significant, the merger ejecta travel homologously keeping the original density profile. The maximum and minimum velocities (corresponding to the velocities at the outermost and innermost radii of the ejecta) are denoted as v_{max} and v_{min} , respectively. Here, we assume that the ejecta is mainly composed of the dynamical ejecta with a power-law density profile described by

$$\rho(r, t) = \frac{f(\beta, v_{\text{max}}/v_{\text{min}}) M_e}{4\pi\Omega R_{\text{in}}^3} \left(\frac{r}{R_{\text{in}}}\right)^{-\beta}, \quad (16)$$

where $f(\beta, v_{\text{max}}/v_{\text{min}}) = (\beta - 3)/[1 - (v_{\text{max}}/v_{\text{min}})^{3-\beta}]$ is the normalization factor of the density, and $R_{\text{in}} (= v_{\text{min}}t)$ is the inner radius of the ejecta. Numerical simulations suggest that the index β has a range of $3 \lesssim \beta \lesssim 4$ (Hotokezaka et al. 2013; Nagakura et al. 2014).

We define two characteristic radii. One is the diffusion radius R_{diff} , where the dynamical time is equal to the diffusion time, and the photospheric radius R_{ph} , where the optical depth τ is unity. The optical depth at a radius r is evaluated by¹⁰

$$\tau(r) = \int_r^{2r} \kappa_e \rho dr' = \frac{f\kappa_e M_e}{4\pi\Omega R_{\text{in}}^2} \frac{1 - 2^{1-\beta}}{\beta - 1} \left(\frac{r}{R_{\text{in}}}\right)^{1-\beta} \quad (17)$$

The diffusion radius at time t is given by

$$R_{\text{diff}} = \frac{c}{\tau(R_{\text{diff}})} t. \quad (18)$$

Then, we obtain the diffusion radius by substituting Eq.

¹⁰ Since we mainly focus on the diffusively thin phase, we do not consider the early time evolution of the radii, where the radii $2R_{\text{diff}}$ and $2R_{\text{ph}}$ are larger than the outer radius $R_{\text{out}} (= v_{\text{max}}t)$, so-called the thin diffusion phase (Kisaka et al. 2015).

TABLE 2
THE FIDUCIAL PARAMETERS OF THE COCOON AND THE MERGER EJECTA FOR MODEL (A) IN TABLE 1.

	Symbol	Cocoon	Merger Ejecta
Opacity times Mass	κM	$0.0025 \text{ cm}^2 \text{ g}^{-1} M_\odot$	$0.03 \text{ cm}^2 \text{ g}^{-1} M_\odot$
Velocity	$v_c, v_{\text{max/min}}$	$0.3 c$	$0.1 - 0.4 c$
Subtended Solid Angle	Ω	0.5	0.5
Power Law Index of Density Profile	β	-(one-zone)	3.5
Injection Energy times Time	$E_{\text{in}} t_{\text{in}}$	10^{52} erg s	-
X-ray Excess Luminosity	$L_X(t)$	-	$8 \times 10^{41} (t/\text{day})^{-1.3} \text{ erg s}^{-1}$

Notes. The ejecta mass should be smaller than that required in the r -process model ($M_c \lesssim 0.02 M_\odot$ and $M_e \lesssim 0.03 M_\odot$) in order to neglect the r -process heating.

(17) into Eq. (18),

$$R_{\text{diff}} = R_{\text{in}} \left[\frac{f(1 - 2^{1-\beta})}{\beta - 1} \frac{\kappa_e M_e}{4\pi v_{\text{min}} c t^2} \right]^{\frac{1}{\beta-2}} \propto t^{\frac{\beta-4}{\beta-2}}. \quad (19)$$

The photosphere is given by equating Eq. (17) with unity,

$$R_{\text{ph}} = R_{\text{in}} \left[\frac{f(1 - 2^{1-\beta})}{\beta - 1} \frac{\kappa_e M_e}{4\pi \Omega v_{\text{min}}^2 t^2} \right]^{\frac{1}{\beta-1}} \propto t^{\frac{\beta-3}{\beta-1}}. \quad (20)$$

We estimate the times t_{diff} and t_{tr} when the diffusion and photospheric radii reach the innermost ejecta radius, respectively. Each timescale corresponds to the diffusion time and the transparent timescale discussed in section 2. By equating the diffusion radius and the photosphere with the innermost radius of ejecta, we get

$$t_{\text{diff}} = \sqrt{\frac{f(1 - 2^{1-\beta})}{\beta - 1} \frac{\kappa_e M_e}{4\pi \Omega v_{\text{min}} c}}, \quad (21)$$

$$t_{\text{tr}} = \sqrt{\frac{f(1 - 2^{1-\beta})}{\beta - 1} \frac{\kappa_e M_e}{4\pi \Omega v_{\text{min}}^2}}, \quad (22)$$

respectively. As we discussed in section 2, the density structure gives the coefficient $\xi = f(1 - 2^{1-\beta})/(\beta - 1)$, which reduce the timescales about ~ 0.3 from the values given by the one-zone estimation.

When the merger ejecta is diffusively thin and optically thick, $t_{\text{diff}} < t < t_{\text{tr}}$, X-rays radiated from the central engine are absorbed in the ejecta, and reprocessed to lower energy photons with a blackbody spectrum. We should remind that when the ejecta is otherwise diffusively thick, the reprocessed photons can not leak out of the ejecta. Furthermore, it should be noted that the reprocessed photons do not show the thermal spectrum if the ejecta is optically thin. As we discussed in section 2.2.2, from the observation that the red macronova shows spectra deviating from a blackbody at ~ 7 days, the ejecta parameter $\kappa_e M_e$ is constrained as given Eq. (12). This condition is satisfied with reasonable merger ejecta parameters such as $\kappa_e \simeq 10 \text{ cm}^2 \text{ g}^{-1}$ and $M_e \simeq 3 \times 10^{-3} M_\odot$ (see also section 2.1.1). The bolometric light curve of the reprocessed emission follows the irradiation luminosity $L_{\text{bol}}(t) = L_X(t)$. Motivated by the X-ray excess detected in GRB 130603B with power-law temporal decay (Fong et al. 2014), we also assume a power-law-decaying irradiation luminosity of

$$L_X(t) = L_X \left(\frac{t}{\text{day}} \right)^{-\alpha_X}, \quad (23)$$

where L_X is the normalization. The power-law decay might be related with the fallback accretion, whose mass accretion rate would also show the power-law temporal decay with index $\sim 5/3$. We determine the photospheric temperature with Eqs. (15) and (20).

In Fig. 4, we show the light curves of the reprocessed emission from the merger ejecta with solid curves. In Table 2, we show the adopted parameters. The reprocessed emission also shows good agreements with the observed red macronova. We extend the light curves after the merger ejecta becomes optically thin ($t > t_{\text{tr}}$) with thin solid curves, by assuming $R_{\text{ph}} = R_{\text{in}}$ and a blackbody spectrum.

In Fig. 5, we show the bolometric luminosity and temperature with solid red and blue lines, respectively. The magenta data points and dash-dotted line are the isotropic X-ray excess luminosity observed in GRB 130603B taken from Fong et al. (2014), which we convert from the observed flux. We also reduce the X-ray luminosity by multiplying 0.3 to compare with the macronova's bolometric luminosity. The luminosity of the X-ray excess in GRB 130603B has a similar slope to that of the macronova. Note that the temporal index α_X which we adopt (see Table 2) is roughly similar to the index of the fallback accretion, $5/3 \simeq 1.67$, and the index of the X-ray excess in GRB 130603B, $\simeq 1.3$ (Fong et al. 2014). Smartt et al. (2017) show that the light curve is fitted by choosing the temporal index $\sim 1.2 \pm 0.3$, which is favored by the r -process heating. While they conclude that SSS17a may be powered by the radioactive decay heating by r -process elements, our result suggests another possibility, i.e., the engine-powered macronova.

As shown in Fig. 4, the reprocessed emission lasts for $t_{\text{diff}} < t < t_{\text{tr}}$ and the light curves do not connect with the light curves of the jet-powered cocoon. This is natural because we consider only two component (two combinations of κM) discrete ejecta. In the realistic situation, there should be a gradient of the opacity ($0.1 \lesssim \kappa/\text{cm}^2 \text{ g}^{-1} \lesssim 10$) or the ejecta mass, and fill the gap in the both light curves smoothly. Furthermore, the reprocessed emission rises at $t \lesssim t_{\text{diff}}$, and this also fills up the gap.

3.2.2. Reprocessed Emission from Cocoon

Finally, we discuss the reprocessed emission from the cocoon when the cocoon does not receive a significant energy injection from jet activities (model (B)). Here, we simply calculate the emission by using a one-zone model as in section 3.1. We derive the temporal evolution of the photospheric radius by solving,

$$1 = \tau = \kappa \rho \Delta R, \quad (24)$$

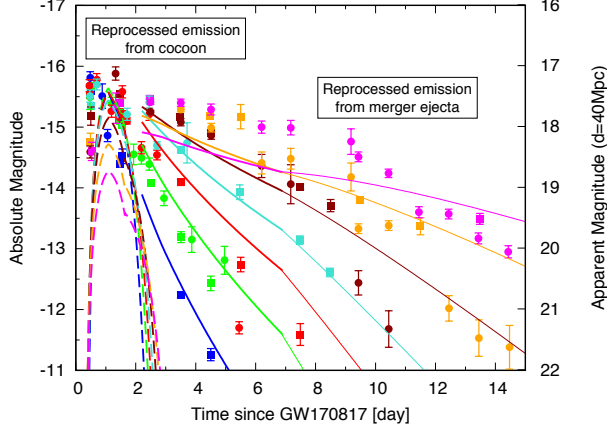


FIG. 6.— The same as Fig. 4 but for model (B). Both blue and red macronovae are powered by the reprocessed emissions from the cocoon (solid) and the merger ejecta (dashed), respectively.

where $\Delta R = R - R_{\text{ph}}$. The photospheric radius is obtained as

$$R_{\text{ph}} = R \left(1 - \frac{t^2}{t_{\text{tr}}^2} \right), \quad (25)$$

which shows that the photosphere shrinks at later time $t \sim t_{\text{tr}}$. However, the cocoon may have a complex density structure in the innermost region due to the mixing or shock interactions with the merger ejecta. In particular, before the photosphere reaches the innermost radius of the cocoon ($R_{\text{ph}} \rightarrow 0$), the one-zone approximation breaks down. Therefore, we assume that the innermost radius of the cocoon is roughly equal with that of the merger ejecta R_{in} . We also depict the light curve for $t < t_{\text{diff}}$ and $t \gtrsim t_{\text{tr}}$ by suppressing the irradiation luminosity with exponential cut-offs.

In Fig. 6, we show the light curves of the reprocessed emission from the cocoon in addition to those of the merger ejecta (model (B)). Both light curves are drawn by using a single X-ray excess luminosity with the same function form of Eq. (23). We adopt the same ejecta parameters as in Fig. 4, but the X-ray luminosity of $L_X(t) = 7 \times 10^{41} (t/\text{day})^{-1.3} \text{ erg s}^{-1}$. The cocoon parameters are the same as the values in Table 2, which satisfy the observational constraint of $t_{\text{diff}} \lesssim 1 \text{ day}$ (see also Eq. (5)). The reprocessed emission from the cocoon has a rather higher temperature than the observed one because in the one-zone model, the photosphere just recedes, which raises the photospheric temperature. In order to obtain more detailed temporal behavior of the photosphere, we should consider the density structure of the cocoon. It should be noted again that the gap between the light curves of the cocoon and the merger ejecta is filled up by the emission from the ejecta with κM connecting the value of the cocoon and the merger ejecta (section 3.2).

4. DISCUSSION

In this work, we study whether the energy injection from the central engine rather than the r -process radioactive decay can produce the observed blue and red macronova emissions or not. Since in the engine model, only the product of the ejecta mass and opacity κM is

constrained by the observed emission timescale, large parameter spaces are allowed (see Figs. 1 and 2). The observations suggest that the ejecta has a polar or radial distribution of κM from $\kappa M \simeq 2 \times 10^{-3} \text{ cm}^2 \text{ g}^{-1} M_{\odot}$ (with $v \simeq 0.3 c$ for the blue macronova at 1 day, see Eq. (5)) to $\kappa M \simeq 3 \times 10^{-2} \text{ cm}^2 \text{ g}^{-1} M_{\odot}$ (with $v \simeq 0.1 c$ for the red macronova at 1 week, see Eq. (12)). We can consider various possible configurations of ejecta and energy sources (see Table 1). In particular, we depict light curves based on two models in section 3. In model (A), we consider jet activities and X-rays from the matter fallback as energy sources. While the jet activities inject energy into a cocoon, the X-rays are absorbed by merger ejecta and reprocessed into NIR photons. In model (B), both the cocoon and merger ejecta are irradiated by X-rays to power reprocessed emissions. With reasonable amounts of the injection energy, the diffusion or reprocessed emission from the cocoon and the reprocessed emission from the merger ejecta reproduce the observed blue and red macronovae, respectively. The reprocessed emission of the X-rays is motivated by the observed X-ray excess in GRB 130603B, which can explain the luminosity and duration of the NIR macronova associated with GRB 130603B with a single energy source, i.e., the central engine. With the polar distributions of the ejecta mass or opacity, even a single-component ejecta can reproduce the observed blue and red macronovae in the engine model (models (C) and (D)).

The necessary mass in the engine model can be smaller than that required by the r -process model (see Fig. 1 and 2). As long as the products κM are fixed, we can adopt various values of opacity and ejecta mass. In particular, as shown in Figs. 4 and 5, the engine model can reproduce the observed blue and red macronovae with the ejecta mass of $M_{\text{ej}}^{\text{blue}} = M_c \simeq 0.005 M_{\odot} (\kappa_c/0.5 \text{ cm}^2 \text{ g}^{-1})^{-1}$ and $M_{\text{ej}}^{\text{red}} = M_e \simeq 0.003 M_{\odot} (\kappa_e/10 \text{ cm}^2 \text{ g}^{-1})^{-1}$, respectively. On the other hand, the r -process model requires more mass of $M_{\text{ej}}^{\text{blue}}, M_{\text{ej}}^{\text{red}} \gtrsim 0.02 - 0.03 M_{\odot}$. The smaller ejecta mass than that in the r -process model can resolve the concerns which we raise in section 1.

Although we illustrate the above ejecta mass and opacity values motivated by numerical simulations, the different values can be also allowed. Then, we can discuss the minimum required mass or opacity by fixing the other parameter values. For the jet-powered cocoon, if the ejecta have significant r -process elements $\kappa_c \simeq 10 \text{ cm}^2 \text{ g}^{-1}$, only a small amount of ejecta mass $M_c \simeq 3 \times 10^{-4} M_{\odot}$ is sufficient to power the blue macronova. In this case, the injection energy should be smaller than the ejecta's kinetic energy $\sim 10^{49} \text{ erg}$. Then, since the required injection energy is $E_{\text{in}} t_{\text{in}} = 10^{52} \text{ erg s}$ (see Table 2), only plateau emissions ($t_{\text{in}} > 10^3 \text{ s}$) could reproduce the observed blue macronova. If future radio observations will give a constraint on the ejecta mass ($\lesssim 10^{-3} M_{\odot}$), the blue macronova strongly supports the existence of the long-timescale engine activity in sGRB 170817A.

As we discuss in the previous sections, while the r -process elements may not be essential as an energy source, they are likely an opacity source. By considering a reasonable range of the merger ejecta mass, we can show that the r -process elements may be necessary to explain the observed emission timescale. Re-

regardless of the energy source, e.g., the r -process heating or the central engine, photons should be thermalized to the NIR energy in the ejecta. Therefore, at least a part of the ejecta should be optically thick to NIR photons, and the emission time has to satisfy the condition, $t < t_{\text{tr}} \simeq 12.4 \text{ day } \kappa_{e,10}^{1/2} M_{e,0.01}^{1/2} v_{e,0.1}^{-1} \Omega_{0.5}^{-1/2} (\xi/0.026)^{1/2}$. Even for a large mass ejecta of $M_e = 0.1 M_\odot$, this condition requires the large opacity as

$$\kappa_e > 0.31 \text{ cm}^2 \text{ g}^{-1} \left(\frac{t}{7 \text{ day}} \right)^2 \left(\frac{v_{\text{min}}}{0.1 c} \right)^2 \left(\frac{M_e}{0.1 M_\odot} \right)^{-1} \Omega_{0.5} \left(\frac{\xi}{0.026} \right)^{-1}, \quad (26)$$

where the velocity v_{min} is not able to be changed a lot. While this constraint is not so strong as to require r -process elements definitely, it is easily satisfied by the small amount of r -process elements (Lanthanoids, Kasen et al. 2013; Tanaka & Hotokezaka 2013; Tanaka et al. 2017). Thus, the strongest evidence of the r -process elements so far is the long duration of the red macronova emission, neither the temporal index of the bolometric light curve, which may be reproduced by the energy injection from the X-ray excess, nor the spectral lines, for which there remain theoretical uncertainties. We remark that other than the r -process elements, dust grains are also proposed as an opacity source (Takami et al. 2014). However, the observed line feature in the spectrum (Chornock et al. 2017; Kilpatrick et al. 2017; Nicholl et al. 2017; Pian et al. 2017; Shappee et al. 2017) may not prefer this possibility (see also, Gall et al. 2017).

The merger ejecta satisfying Eq. (12) becomes optically thin ~ 7 days after the merger ($t > t_{\text{tr}}$). In this case, the reprocessed photons are not thermalize completely, and may show deviations from the thermal spectrum in bluer wavelength. In the observations of SSS17a, the spectra actually deviate from a blackbody at late time. While these spectra are roughly fitted in the r -process model (Chornock et al. 2017; Kilpatrick et al. 2017; Nicholl et al. 2017; Pian et al. 2017; Shappee et al. 2017), we could also fit them in the engine model. In order to predict the non-thermalized spectrum, we need a detailed radiative transfer calculation, which is beyond the scope of this paper. This is an interesting future problem to compare the spectra given by both models

and clarify whether macronovae are produced by the energy injection from the central engine or not.

In addition to late-time spectra, light curves at the early phase may be useful to study what powers macronovae. While the r -process heating rate is well understood, various energy injection processes are possible in the engine model. Therefore, the difference of the heating mechanisms may be reflected in the early-time light curves ($t \lesssim 1$ day, see e.g., Fig. 6 in Kisaka et al. 2015).

The observed macronova shows a smooth bolometric light curve for $\sim 1 - 7$ days (Smartt et al. 2017; Waxman et al. 2017). Thus, the single-energy-source scenario (models (B)-(D)) can more naturally reproduce the observed light curve than the double-energy-source scenario (model (A)). Although reasonable jet parameters gives the diffusion luminosity comparable to the reprocessed emission in model (A), the possible injected energy by jets has a relatively broad range. Then, the detection of very bright blue macronovae which requires too much mass to explain the event in the r -process model, can be a smoking gun of the engine model (for the case of model (A)).

Murase et al. (2017) discuss high energy emissions from the merger remnant at late time. They find that if a super Eddington accretion disk with luminosity $L_X \sim 10^{40} \text{ erg s}^{-1}$ exists as a merger remnant, X-rays from the disk can escape from the ejecta at 30 – 100 days after the merger. *NuSTAR* gives an interesting upper limit at $\simeq 30$ days (Evans et al. 2017) and rejects the disk luminosity of $L_X \gtrsim 10^{41} \text{ erg s}^{-1}$. The late-time X-ray observation (Ruan et al. 2017) also rejects the possibility that the central engine powers the X-ray emission (Margutti et al. 2018). The X-ray irradiation luminosity we assume (see, Table 2), becomes $L_X \sim 10^{38-39} \text{ erg s}^{-1}$ at 30 – 100 days, which is consistent with these *NuSTAR* and *Chandra* observation.

We thank Masaru Shibata and Masaomi Tanaka for useful comments and discussions. TM thank Sho Fujibayashi for fruitful discussions in public baths nearby Kyoto University. This work is supported by Grant-in-Aid for JSPS Research Fellow 17J09895 (TM) and KAKENHI 24103006, 26247042, 26287051, 17H01126, 17H06131, 17H06357, 17H06362 (KI), and 16J06773 (SK).

REFERENCES

- Abbott, B. P., Abbott, R., Abbott, T. D., et al. 2017, *Physical Review Letters*, 119, 161101
- Alexander, K. D., Berger, E., Fong, W., et al. 2017, *ApJ*, 848, L21
- Arcavi, I., Hosseinzadeh, G., Andrew Howell, D., et al. 2017, *Nature*, 541
- Arnett, W. D. 1980, *ApJ*, 237, 541
- Barthelmy, S. D., Cannizzo, J. K., Gehrels, N., et al. 2005, *ApJ*, 635, L133
- Berger, E., Fong, W., & Chornock, R. 2013, *ApJ*, 774, L23
- Ciolfi, R., Kastaun, W., Giacomazzo, B., et al. 2017, *Phys. Rev. D*, 95, 063016
- Cowperthwaite, P. S., Berger, E., Villar, V. A., et al. 2017, *ApJ*, 848, L17
- Dessart, L., Ott, C. D., Burrows, A., Rosswog, S., & Livne, E. 2009, *ApJ*, 690, 1681
- Díaz, M. C., Macri, L. M., Garcia Lambas, D., et al. 2017, *ApJ*, 848, L30
- Dietrich, T., Ujevic, M., Tichy, W., Bernuzzi, S., & Brügmann, B. 2017, *Phys. Rev. D*, 95, 024029
- Chornock, R., Berger, E., Kasen, D., et al. 2017, *ApJ*, 848, L19
- Coulter, D. A., Foley, R. J., Kilpatrick, C. D., et al. 2017, *Science*
- Drout, M. R., Piro, A. L., Shappee, B. J., et al. 2017, *Science*
- Eichler, D., Livio, M., Piran, T., & Schramm, D. N. 1989, *Nature*, 340, 126
- Evans, P. A., Cenko, S. A., Kennea, J. A., et al. 2017, *Science*
- Fernández, R., & Metzger, B. D. 2013, *MNRAS*, 435, 502
- Fernández, R., Kasen, D., Metzger, B. D., & Quataert, E. 2015, *MNRAS*, 446, 750
- Fernández, R., Quataert, E., Schwab, J., Kasen, D., & Rosswog, S. 2015b, *MNRAS*, 449, 390
- Fong, W., Berger, E., Metzger, B. D., et al. 2014, *ApJ*, 780, 118

- Fong, W., Berger, E., Margutti, R., & Zauderer, B. A. 2015, *ApJ*, 815, 102
- Fong, W., Margutti, R., Chornock, R., et al. 2016, *ApJ*, 833, 151
- Fong, W., Berger, E., Blanchard, P. K., et al. 2017, *ApJ*, 848, L23
- Fujibayashi, S., Sekiguchi, Y., Kiuchi, K., & Shibata, M. 2017, *ApJ*, 846, 114
- Fujibayashi, S., Kiuchi, K., Nishimura, N., Sekiguchi, Y., & Shibata, M. 2017b, arXiv:1711.02093
- Gall, C., Hjorth, J., Rosswog, S., Tanvir, N. R., & Levan, A. J. 2017, *ApJ*, 849, L19
- Giacomazzo, B., Zrake, J., Duffell, P. C., MacFadyen, A. I., & Perna, R. 2015, *ApJ*, 809, 39
- Goldstein, A., Veres, P., Burns, E., et al. 2017, *ApJ*, 848, L14
- Gompertz, B. P., O'Brien, P. T., Wynn, G. A., & Rowlinson, A. 2013, *MNRAS*, 431, 1745
- Gompertz, B. P., O'Brien, P. T., & Wynn, G. A. 2014, *MNRAS*, 438, 240
- Gompertz, B. P., Levan, A. J., Tanvir, N. R., et al. 2017, arXiv:1710.05442
- Gottlieb, O., Nakar, E., & Piran, T. 2017, arXiv:1705.10797
- Gottlieb, O., Nakar, E., Piran, T., & Hotokezaka, K. 2017b, arXiv:1710.05896
- Haggard, D., Nynka, M., Ruan, J. J., et al. 2017, *ApJ*, 848, L25
- Hallinan, G., Corsi, A., Mooley, K. P., et al. 2017, *Science*
- Hotokezaka, K., Kiuchi, K., Kyutoku, K., et al. 2013, *Phys. Rev. D*, 87, 024001
- Ioka, K., Kobayashi, S., & Zhang, B. 2005, *ApJ*, 631, 429
- Ioka, K., & Nakamura, T. 2017, arXiv:1710.05905
- Jin, Z.-P., Hotokezaka, K., Li, X., et al. 2016, *Nature Communications*, 7, 12898
- Kasen, D., Badnell, N. R., & Barnes, J. 2013, *ApJ*, 774, 25
- Kasen, D., Metzger, B., Barnes, J., et al. 2017, *Nature*
- Kasliwal, M. M., Nakar, E., Singer, L. P., et al. 2017, *Science*
- Kilpatrick, C. D., Foley, R. J., Kasen, D., et al. 2017, *Science*
- Kisaka, S., & Ioka, K. 2015, *ApJ*, 804, L16
- Kisaka, S., Ioka, K., & Takami, H. 2015, *ApJ*, 802, 119
- Kisaka, S., Ioka, K., & Nakar, E. 2016, *ApJ*, 818, 104
- Kisaka, S., Ioka, K., & Sakamoto, T. 2017, *ApJ*, 846, 142
- Kiuchi, K., Kyutoku, K., Sekiguchi, Y., Shibata, M., & Wada, T. 2014, *Phys. Rev. D*, 90, 041502
- Kiuchi, K., Sekiguchi, Y., Kyutoku, K., et al. 2015, *Phys. Rev. D*, 92, 064034
- Kulkarni, S. R. 2005, arXiv:astro-ph/0510256
- Kyutoku, K., Ioka, K., & Shibata, M. 2014, *MNRAS*, 437, L6
- Lattimer, J. M., & Schramm, D. N. 1974, *ApJ*, 192, L145
- Lazzati, D., Perna, R., Morsony, B. J., et al. 2017, arXiv:1712.03237
- Li, L.-X., & Paczyński, B. 1998, *ApJ*, 507, L59
- Lippuner, J., Fernández, R., Roberts, L. F., et al. 2017, *MNRAS*, 472, 904
- LIGO Scientific Collaboration & Virgo Collaboration, et al. 2017, *ApJ*, 848, L12
- LIGO Scientific Collaboration & Virgo Collaboration, et al. 2017b, *ApJ*, 848, L13
- Margutti, R., Berger, E., Fong, W., et al. 2017, *ApJ*, 848, L20
- Margutti, R., Alexander, K. D., Xie, X., et al. 2018, arXiv:1801.03531
- Matsumoto, T., Nakauchi, D., Ioka, K., & Nakamura, T. 2016, *ApJ*, 823, 83
- Metzger, B. D., Martínez-Pinedo, G., Darbha, S., et al. 2010, *MNRAS*, 406, 2650
- Metzger, B. D., & Fernández, R. 2014, *MNRAS*, 441, 3444
- Metzger, B. D., & Piro, A. L. 2014, *MNRAS*, 439, 3916
- McCully, C., Hiramatsu, D., Andrew Howell, D., et al. 2017, *ApJ*, 848, L32
- Mooley, K. P., Nakar, E., Hotokezaka, K., et al. 2017, arXiv:1711.11573
- Murase, K., Toomey, M. W., Fang, K., et al. 2017, arXiv:1710.10757
- Murguia-Berthier, A., Ramirez-Ruiz, E., Kilpatrick, C. D., et al. 2017, *ApJ*, 848, L34
- Nakar, E., & Piran, T. 2017, *ApJ*, 834, 28
- Nakar, E., & Piran, T. 2018, arXiv:1801.09712
- Nagakura, H., Hotokezaka, K., Sekiguchi, Y., Shibata, M., & Ioka, K. 2014, *ApJ*, 784, L28
- Nicholl, M., Berger, E., Kasen, D., et al. 2017, *ApJ*, 848, L18
- Perego, A., Rosswog, S., Cabezón, R. M., et al. 2014, *MNRAS*, 443, 3134
- Pian, E., D'Avanzo, P., Benetti, S., et al. 2017, *Nature*, 551, 67
- Piro, A. L., & Kollmeier, J. A. 2017, arXiv:1710.05822
- Price, D. J., & Rosswog, S. 2006, *Science*, 312, 719
- Qian, Y.-Z. 2000, *ApJ*, 534, L67
- Rossi, E. M., & Begelman, M. C. 2009, *MNRAS*, 392, 1451
- Rosswog, S. 2007, *MNRAS*, 376, L48
- Ruan, J. J., Nynka, M., Haggard, D., Kalogera, V., & Evans, P. 2017, arXiv:1712.02809
- Savchenko, V., Ferrigno, C., Kuulkers, E., et al. 2017, *ApJ*, 848, L15
- Sekiguchi, Y., Kiuchi, K., Kyutoku, K., & Shibata, M. 2015, *Phys. Rev. D*, 91, 064059
- Sekiguchi, Y., Kiuchi, K., Kyutoku, K., Shibata, M., & Taniguchi, K. 2016, *Phys. Rev. D*, 93, 124046
- Shappee, B. J., Simon, J. D., Drout, M. R., et al. 2017, *Science*
- Shibata, M., Kiuchi, K., & Sekiguchi, Y.-i. 2017, *Phys. Rev. D*, 95, 083005
- Shibata, M., Fujibayashi, S., Hotokezaka, K., et al. 2017b, arXiv:1710.07579
- Siegel, D. M., & Metzger, B. D. 2017, arXiv:1705.05473
- Smartt, S. J., Chen, T.-W., Jerkstrand, A., et al. 2017, *Nature*
- Soares-Santos, M., Holz, D. E., Annis, J., et al. 2017, *ApJ*, 848, L16
- Symbolist, E., & Schramm, D. N. 1982, *Astrophys. Lett.*, 22, 143
- Takami, H., Nozawa, T., & Ioka, K. 2014, *ApJ*, 789, L6
- Tanaka, M., & Hotokezaka, K. 2013, *ApJ*, 775, 113
- Tanaka, M., Kato, D., Gaigalas, G., et al. 2017, arXiv:1708.09101
- Tanaka, M., Utsumi, Y., Mazzali, P. A., et al. 2017b, *PASJ*
- Tanvir, N. R., Levan, A. J., Fruchter, A. S., et al. 2013, *Nature*, 500, 547
- Tanvir, N. R., Levan, A. J., González-Fernández, C., et al. 2017, *ApJ*, 848, L28
- Tauris, T. M., Kramer, M., Freire, P. C. C., et al. 2017, *ApJ*, 846, 170
- Tominaga, N., Tanaka, M., Morokuma, T., et al. 2017, arXiv:1710.05865
- Troja, E., Piro, L., van Eerten, H., et al. 2017, *Nature*
- Utsumi, Y., Tanaka, M., Tominaga, N., et al. 2017, *PASJ*
- Valenti, S., Sand, D. J., Yang, S., et al. 2017, *ApJ*, 848, L24
- Wanajo, S., & Janka, H.-T. 2012, *ApJ*, 746, 180
- Wanajo, S., Sekiguchi, Y., Nishimura, N., et al. 2014, *ApJ*, 789, L39
- Waxman, E., Ofek, E., Kushnir, D., & Gal-Yam, A. 2017, arXiv:1711.09638
- Yang, B., Jin, Z.-P., Li, X., et al. 2015, *Nature Communications*, 6, 7323
- Yu, Y.-W., & Dai, Z.-G. 2017, arXiv:1711.01898
- Yu, Y.-W., Zhang, B., & Gao, H. 2013, *ApJ*, 776, L40